Three-dimensional organization of active rRNA genes within the nucleolus

Thierry Cheutin[1], Marie-Françoise O'Donohue[1], Adrien Beorchia[2], Marc Vandelaer[3], Hervé Kaplan[4], Bruno Deféver[4], Dominique Ploton[1,*] and Marc Thiry[3]

[1]Unité MéDIAN, CNRS UMR 6142, UFR de Pharmacie, 51 rue Cognacq-Jay, 51096 Reims Cedex, France
[2]DTI, UMR 6107, UFR de Sciences, BP 1039, 51687 Reims Cedex, France
[3]Laboratoire de Biologie Cellulaire et Tissulaire, Université de Liège, 20 rue de Pitteurs, 4020 Liège, Belgium
[4]IFR53, 51 rue Cognacq-Jay, 51096 Reims Cedex, France
*Author for correspondence (e-mail: dominique.ploton@univ-reims.fr)

Accepted 23 May 2002
Journal of Cell Science 115, 3297-3307 (2002) © The Company of Biologists Ltd

Summary

In this work, we have localized transcribing rRNA genes at the ultrastructural level and described their three-dimensional organization within the nucleolus by electron tomography. Isolated nucleoli, which exhibit a reduced transcriptional rate, were used to determine the sites of initial BrUTP incorporation (i.e. rRNA synthesis by the transcriptional machinery). Using pulse-chase experiments with BrUTP and an elongation inhibitor, cordycepin, it was possible to precisely localize the initial sites of BrUTP incorporation. Our data show that BrUTP incorporation initially takes place in the fibrillar centers and that elongating rRNAs rapidly enter the surrounding dense fibrillar component. Furthermore, we investigated the spatial arrangement of RNA polymerase I molecules within the whole volume of the fibrillar centers. Electron tomography was performed on thick sections of cells that had been labeled with anti-RNA polymerase I antibodies prior to embedding. Detailed tomographic analyses revealed that RNA polymerase I molecules are mainly localized within discrete clusters. In each of them, RNA polymerase I molecules were grouped as several coils, 60 nm in diameter. Overall, these findings have allowed us to propose a model for the three-dimensional organization of transcribing rDNA genes within the nucleolus.

Movies available on-line

Key words: Cell nucleolus, RNA polymerase I, Pre-ribosomal RNA, BrUTP incorporation, Electron tomography

Introduction

The rRNA genes of higher eukaryotes occur in multiple, tandemly repeated copies that are separated by non-transcribed 'spacers'. Primary ribosomal transcripts (pre-rRNAs) are synthesized by RNA polymerase I (RPI) and gradually processed to give 18S, 5.8S, and 28S rRNAs, which are finally integrated into the ribosomes (Mélèse and Xue, 1995; Moss and Stefanovsky, 1995). Both transcription and processing take place within the nucleoli, which are composed of three major substructures in mammalian cells: the fibrillar center (FC), the dense fibrillar component (DFC) and the granular component (GC) (Hadjiolov, 1985; Derenzini et al., 1990). During the past decade, many researchers have attempted to correlate these structural features with the nucleolar functions described at the molecular level (Shaw and Jordan, 1995; Thiry and Goessens, 1996; Scheer and Hock, 1999; Olson et al., 2000).

Our present knowledge of the molecular organization of transcribed rRNA genes was mainly established using chromatin spreads (Miller and Beatty, 1969). After hypotonic treatment, each transcribing gene decondenses and appears as a so-called 'Christmas tree', 4.5 to 6 μm in length (Trendelenburg and Puvion-Dutilleul, 1987). This 'Christmas tree' consists of 135 to 180 fibrils of growing pre-rRNAs, each of which is connected to the rDNA axis by a RPI molecule (Reeder and Lang, 1997). By contrast, localization of these 'Christmas trees' relative to the different compartments within the nucleolus has proved to be a complex problem. There is a general consensus that transcription occurs in the fibrillar regions of the nucleolus, but whether it is within the DFC or at the border of the DFC and the FC, or even within the FC, remains a matter of much debate (Goessens, 1976; Fakan, 1978; Scheer and Rose, 1984; Thiry et al., 1985; Dupuy-Coin et al., 1986; Derenzini et al., 1987; Raska et al., 1989; Thiry and Goessens, 1991; Dundr and Raska, 1993; Schöfer et al., 1993; Bréchard et al., 1994; Hozak et al., 1994; Cmarko et al., 1999; Biggiogera et al., 2001).

Recently, we reported a new method for BrUTP incorporation within optimally preserved cells that allowed us to follow the kinetics of rRNA synthesis and maturation (Thiry et al., 2000). The results of this work showed that BrUTP-labelled rRNAs are initially localized both within the FC and the inner part of the DFC. However, the speed of rRNA synthesis in vivo is so high [25-50 nucleotides/second (Grummt, 1978)] that the localization of incorporated BrUTP (or [^{3}H]-UTP) could be representative of both incorporation and accumulation sites. In order to resolve this problem, a model in which the molecular events are slowed down is a prerequisite. In addition, conventional microscopy gives two-dimensional pictures that only account for a partial view of the labelling and do not provide a description of the in situ volumic

organization of the rDNA genes. Clearly, alternative approaches providing three-dimensional information, such as electron tomography, must be performed to answer this biological question (Crowther et al., 1970; Héliot et al., 1997; Baumeister et al., 1999).

In this work, we have studied the precise localization of initial BrUTP incorporation sites at the ultrastructural level. To address this point, we used isolated nucleoli, which (when compared with intact cells) exhibit decreased transcriptional activity (Grummt, 1978; Hadjiolov, 1985). Using a pulse-chase procedure and an elongation inhibitor, we demonstrated that the ribosomal transcripts elongate in the cortex of the FC and then enter into the surrounding DFC. Furthermore, we have immunolabelled RPI molecules prior to embedding in order to study their three-dimensional organization in whole cells. Electron tomography was performed on sections whose thickness (500 nm) is sufficient to visualize entire FCs. This approach revealed that RPI molecules are located within the cortex of the FC, where they are organized within three to five curved coils constituted with bent twines. These results led us to propose a model for the volumic organization of the 'Christmas trees' that reconciles all the previous findings by placing the rDNA genes in the FC and the growing rRNA molecules both in the FC and within the DFC.

Materials and Methods

Cell culture and isolation of nucleoli

Human A549 cells were cultured in Ham F12 (Sigma, St Louis, MO) supplemented with 10% foetal calf serum (Sigma) and 2 mM glutamine at 37°C in an atmosphere enriched with 5% CO_2. Cells were loaded onto glass coverslips at a density of 5×10^4 cells/cm^2 and grown for 72 hours. Hypertetraploid Ehrlich ascite tumor (ELT) cells were cultured as described previously (Lepoint and Bassleer, 1978). Approximately 10^8 ELT cells were scraped off monolayer cultures and harvested in Hanks' balanced salt solution (Gibco BRL, Merelbeke, Belgium). Nucleoli were isolated by sonication and purified on a Percoll cushion as previously described (Vandelaer et al., 1996).

In vitro transcription measured by [^{3}H]-GTP incorporation

Isolated nucleoli from ELT cells were suspended in TS buffer (25% glycerol, 10 mM KCl, 50 mM Tris-HCl, pH 7.0, 5 mM $MgCl_2$, 0.5 mM EGTA, 0.2 mM spermidine, 0.4 mM spermine, 25 U/ml RNase inhibitor) (Roche, Meylan, France), and a set of protease inhibitors (0.75 mM PMSF, 30 μg/ml antipain, 2 μg/ml aprotinin, 100 μg/ml EDTA, 0.5 μg/ml leupeptin, 200 μg/ml Pefabloc®, 30 μg/ml phophoramidon, 5 μg/ml bestatin, 0.7 μg/ml pepstatin, 10 μg/ml E-64 and 10 μg/ml chymostatin) (Roche). Reactions were performed in TS buffer to which 0.2 mM ATP, CTP, UTP or BrUTP (Roche) and 500 dpm/pmol [^{3}H]-GTP (Amersham Pharmacia Biotech, Little Chalfont, UK) were added. After incubation for 1 to 30 minutes at 37°C, the transcription process was stopped by adding 1.6 mg/ml bovine serum albumin (BSA) and 5% trichloroacetic acid (TCA). After 30 minutes on ice and a 6 minute centrifugation at 8000 ***g***, the pellet was washed three times in 5% TCA and centrifuged for 6 minutes at 8000 ***g***. The remaining precipitate was diluted in Ecoscint A (National Diagnostics, Atlanta, GA) and counted in triplicate in a Beckman LS3801 scintillation counter (Beckman Coulter, High Wycombe, UK).

In vitro transcription measured by BrUTP incorporation

Isolated nucleoli from ELT cells were suspended in 500 μl TS buffer containing 0.2 mM ATP, GTP and CTP and 0.4 mM BrUTP (TSB buffer). After incubation for 1 to 120 minutes at 37°C, the transcription process was stopped by adding a fixative solution composed of 4% formaldehyde and 0.1% glutaraldehyde in 0.1 M Sorensen's buffer (pH 7.4). After 60 minutes on ice, the pellet was washed in the same buffer before being dehydrated and embedded in Epikote 812. In other experiments, the nucleoli were suspended in TSB buffer containing either 0.2 μg/ml actinomycin D (Sigma) or 100 μg/ml α-amanitin (Roche). For pulse-chase experiments, the nucleoli were pulse-labelled for 5 minutes or 10 minutes, then centrifuged for 1 minute at 665 ***g*** and washed in 8 ml TS buffer containing 0.4 mM UTP. After centrifugation at 665 ***g*** for 1 minute, they were suspended for 15 or 20 minutes in 500 μl TSB buffer containing 0.4 mM UTP instead of BrUTP before being fixed as described above. Finally, to perform inhibition studies, the nucleoli were suspended at 37°C in TSB buffer containing UTP instead of BrUTP and either 0.4 mM cordycepin-5′triphosphate (Sigma) or 0.2 mM ATP, then incubated for 15 minutes. After, a chase was carried out by incubating the nucleoli in TSB buffer at 37°C for 15 minutes in the presence or absence of cordycepin. Fixation and embedding were performed as described above.

Immunogold labelling of BrUTP nucleotides

Ultrathin sections of nucleoli that had incorporated BrUTP were incubated for 30 minutes in PBS (0.14 M NaCl, 6 mM Na_2HPO_4, 4 mM KH_2PO_4, pH 7.2) containing diluted (1:30) normal goat serum and 1% BSA and then rinsed with PBS containing 1% BSA (PBS-BSA). The sections were then incubated for 4 hours at room temperature with a monoclonal anti-BrdU antibody (Becton Dickinson, Franklin Lakes, NJ) diluted 1:50 in PBS and containing 0.2% BSA and diluted (1:50) normal goat serum. After washing with PBS-BSA, the sections were incubated at room temperature for 1 hour with goat anti-mouse IgG coupled to colloidal gold particles, 10 nm in diameter (Janssen Life Sciences, Beerse, Belgium), diluted 1:40 with PBS (pH 8.2) containing 0.2% BSA. After washing with PBS-BSA, the sections were rinsed in deionized water. Finally, the ultrathin sections were mounted on nickel grids and stained with uranyl acetate and lead citrate before examination in a Jeol CX 100 electron microscope at 60 kV (Jeol, Brussels, Belgium). Three kinds of control experiments were carried out: (i) the primary antibody was omitted; (ii) the sections were incubated with antibody-free gold particles; and (iii) BrUTP was replaced by UTP in the transcription buffer.

Quantitative evaluations of colloidal gold particles on ultrathin sections

To evaluate the labelling density, the area of each compartment was first estimated morphometrically by the point-counting method (Weibel et al., 1969). Gold particles were counted from 7 to 15 random micrographs (for the time-course of BrUTP incorporation and effect of actinomycin D) or from 13 to 25 random micrographs (for pulse-chase experiments and studies performed in the presence of cordycepin). After evaluating the areas (Sa) occupied by the various compartments, the number of gold particles (Ni) over each compartment was determined and the labelling density (Ns=Ni/Sa) was calculated. The numerical data obtained do not reflect the exact amounts of BrUTP molecules in the compartments but rather their relative density. For this reason, all specimens in comparative studies were submitted to identical fixation and embedding conditions, and incubation of the different sections was performed simultaneously.

Immunostaining of RPI before embedding

A549 cells were fixed for 10 minutes in 3% paraformaldehyde diluted in PBS, then permeabilized with 0.3% Triton X-100 in PBS for 2 minutes. Cells were soaked for 30 minutes in 3% BSA in PBS, then

incubated for 4 hours with a rabbit polyclonal antibody directed against the large subunit of RPI (a gift from K. Rose, Houston, TX) diluted 1:400. After a 30 minute incubation with a biotinylated goat anti-rabbit antibody (Sigma), the secondary antibody was revealed with fluoronanogold streptavidin (Nanoprobes, New York, USA). The cells were fixed again with 1.6% glutaraldehyde in PBS, washed in deionised water and amplified with HQ silver (Nanoprobes) in order to obtain 10 nm particles. Cells were then harvested by scraping, dehydrated in graded alcohols and embedded in Epikote 812. Ultrathin sections (80 nm) mounted on copper grids were stained with uranyl acetate and lead citrate before examination using a Jeol 200 CX microscope at 80 kV (Jeol).

Electron tomography

500 nm thick sections prepared from A549 cells labelled with anti-RPI antibodies were observed in a medium-voltage CM30 electron microscope working at 250 kV in the STEM mode (Philips, Eindhoven, The Netherlands) (Beorchia et al., 1992). In order to get a high contrast, these sections were not counterstained. Before initiating a tilt series, the section was stabilized under the electron beam at a dose of 100 $e^{-}/(Å^2 \times seconds)$ for 10 minutes to limit anisotropic thinning of the specimen during data collection. Each section was tilted every 2° from –50° to +50°. The 51 corresponding images (512×512 pixels) were recorded directly on a disk-type scintillator-photomultiplier detector system and digitized on-line using Orion hardware (ELI sprl, Belgium). Images were then aligned individually by using a sinogram technique (Bahr et al., 1979). In order to study individual clusters in more detail, the corresponding part of the image was isolated from the original image, resampled and finally realigned. Tomographic reconstruction was performed by using an extended field-additive algorithm-reconstruction technique on aligned images, as previously described (Héliot et al., 1997). Extensive investigations were performed by using the Analyze Software package (Mayo BIR, CN Software, Southwater, UK) and the Amira software (TGS Europe, Mérignac, France) on the reconstructed volumes of 16 clusters taken from different cells. Three-dimensional visualizations with a high depth of field were calculated to obtain pertinent images at fixed angles of view and rotations around any chosen axis. Complex movements around the volumes were also performed, as shown in the movies (available at jcs.biologists.org/supplemental). Finally, the inner parts of the volumes were investigated by presenting sections performed in any chosen plane. For Fig. 8, sections, stereo-pairs and movies were performed after a 2×2×2 downsampling.

Quantification of the labelling density within thick sections

Images of seven 500 nm thick sections obtained from A549 cells labelled with anti-RPI antibodies before embedding were used to quantify the density of the labelling within different parts of the nucleus. By using Metamorph software (Roper Scientific, France), a circle 270 nm in diameter was positioned on 90 different zones of the image (30 outside of the cell, 30 on the nucleoplasm and 30 on clusters), and we measured the density of the labelling for each case. After subtracting the value of the density measured outside of the cell from that of the nucleoplasm and the clusters, the ratio of the labelling density within clusters was calculated relatively to the density within nucleoplasm.

Quantification of the number of active rDNA genes per fibrillar center in A549 cells

Control and DRB-treated A549 cells (100 μg/ml for 6 hours) were fixed for 10 minutes in 3% paraformaldehyde diluted in PBS, then permeabilized with 0.3% Triton X-100 in PBS for 2 minutes. Cells were then immunolabelled with UBF antibody, and a series of optical sections were obtained by confocal microscopy as previously described (Klein et al., 1998). Processing was performed using the Analyze computer software (CNSoftware, Southwater, UK) working on a Sun Sparc20 (Sun Microsystems, Mountain View, CA) workstation. Volumes were isotropically restored to obtain the same pixel size in x, y, z directions. A 3×3×3 cubic median filter was applied to decrease noise, and local enhanced contrast was achieved using Bengali-Le Negrate's method (Le Negrate et al., 1992). After, volumes were binarised. Finally, the number of objects contained within a volume were estimated using three-dimensional quantification software [Analyze package; Qt software (Klein et al., 1998)].

Results

Rate of transcription in isolated nucleoli

The transcription rate within nucleoli isolated from ELT cells was estimated by following [^{3}H]-GTP incorporation and comparing it to that obtained when BrUTP replaced UTP (data not shown). In the presence of the natural precursors, [^{3}H]-GTP incorporation increased rapidly over a 16 minute period and then increased more slowly up to 30 minutes. When BrUTP replaced UTP as a precursor, the transcription rate increased during the first 8 minutes and then reached a plateau. This plateau was maintained during at least 30 minutes at a value that was approximately 40% of that obtained in the presence of UTP.

Sites of BrUTP incorporation in isolated nucleoli

Isolated nucleoli from ELT cells were incubated in the presence of BrUTP for 1, 5, 10 and 25 minutes. The distribution of BrRNAs among the different nucleolar compartments was subsequently visualized and quantified after immunogold labelling with 10 nm gold particles (Fig. 1). The three main nucleolar components (FC, DFC and GC) were easily identified, attesting that the nucleolar ultrastructure was preserved. BrUTP incorporation was rapid (62% and 82% of nucleoli were labelled after 1 and 5 minutes, respectively), with 92-97% of nucleoli being labelled after 10 minutes. Within nucleoli, labelling was observed on the two fibrillar components (FC and DFC) but almost never on the GC or on nucleolus-associated condensed chromatin. Closer examination revealed that on the FC, gold particles were preferentially localized in the cortical regions near to the surrounding DFC (Fig. 1A,B). Quantification of labelling over a 1 to 25 minute period revealed that labelling density was progressively increased on both the FC and the DFC as a function of time (Fig. 2). In addition, labelling density was significantly higher on the FC than on the DFC (with the particle density on the FC and DFC being significantly higher than that in resin). In the presence of a concentration of actinomycin D that inhibits nucleolar transcription, labelling was strongly reduced on all the nucleolar components (Fig. 3). By contrast, in the presence of α-amanitin (an extranucleolar transcriptional inhibitor), no reduction of the nucleolar labelling was observed (data not shown).

Localization of elongating rRNAs by pulse-chase

In order to determine whether pre-rRNAs enter new compartments during the elongation process, the distribution

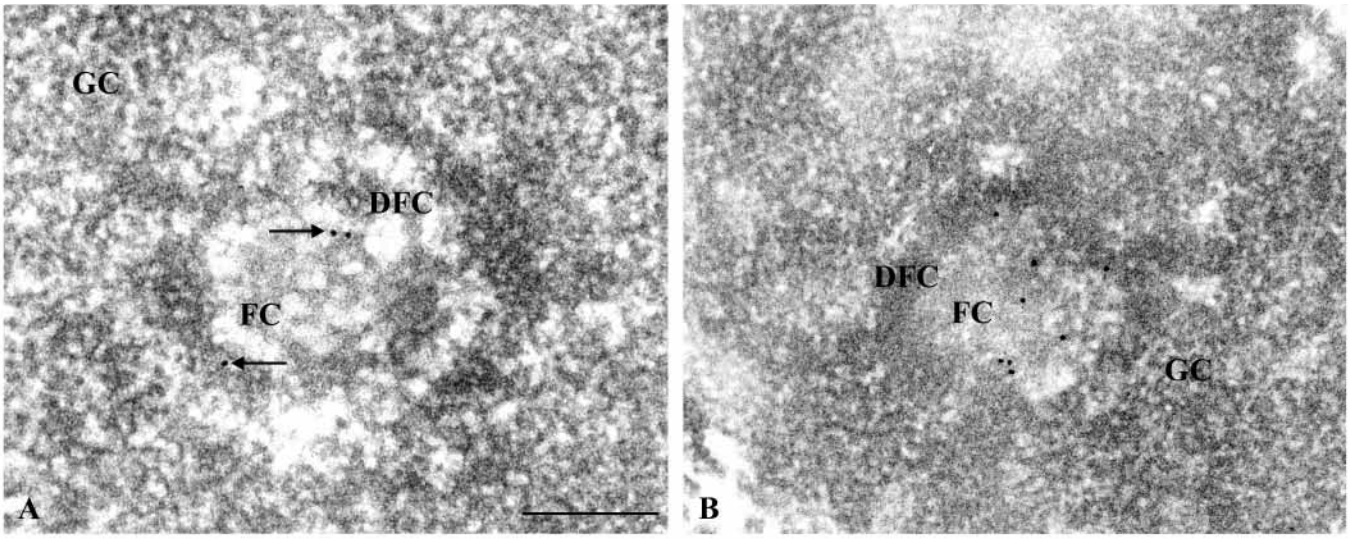

Fig. 1. Ultrastructural localization of nascent rRNA molecules within the nucleolus. Immunogold labelling detection of BrUTP-labelled rRNAs on ultrathin sections of isolated nucleoli from ELT cells pulse-labelled for 1 minute (A) and 10 minutes (B). The main nucleolar components are clearly identified: fibrillar centers (FC), dense fibrillar component (DFC) and granular component (GC). Arrows in (A) point to gold particles. Bar, 0.25 μm.

of labelling was analysed in isolated nucleoli submitted to a 10 minute pulse with BrUTP, followed by an optional 20 minute chase with UTP. In both cases, labelling was consistently present on the fibrillar components (data not shown). Gold particles were mainly observed on the cortical part of the FC, whereas its central part was almost devoid of labelling. However, relative to the FC, labelling density was higher on the DFC after the chase. A quantitative evaluation revealed that the labelling density on the FC was significantly higher than that on the DFC in the pulse experiment (Fig. 4). A 5 minute pulse followed by a 15 minute chase led to similar results (data not shown).

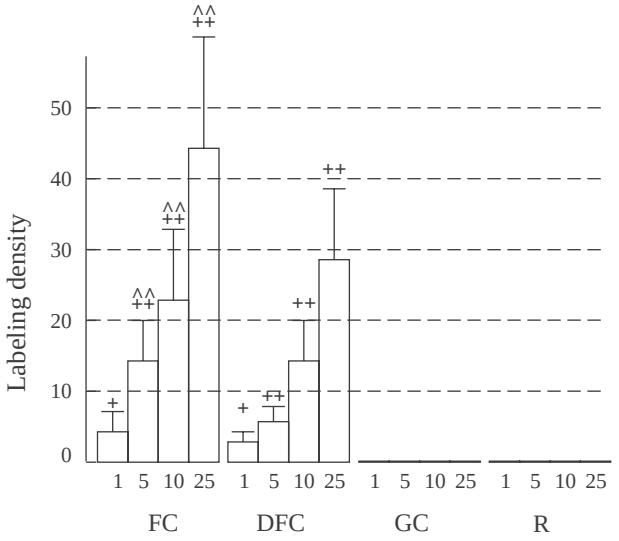

Fig. 2. Densities (gold particles/μm^2) on the FC, DFC, GC and resin (R) in nucleoli isolated from ELT cells and incubated with BrUTP for 1 to 25 minutes. The results shown represent mean values±s.e.m. 7, 14, 13 and 12 random micrographs were analyzed and 51, 120, 211 and 274 gold particles were counted, respectively. Student's *t*-test for nucleolar components versus resin (+ P<0.05, ++ P<0.01) and for FC versus DFC in different pulse-labelled nucleoli (^ P<0.05, ^^ P<0.01) was used.

Identification of the initial sites of rRNA elongation

In this experiment, isolated nucleoli were incubated with BrUTP after a transient inhibition of elongation by cordycepin, which leads to premature transcription termination and release of incomplete transcripts from their templates (Siev et al., 1969; Suhadolnik, 1979). After the release of inhibition, RPI molecules are immediately re-engaged in transcription, and this allows us to identify the initial sites of BrUTP

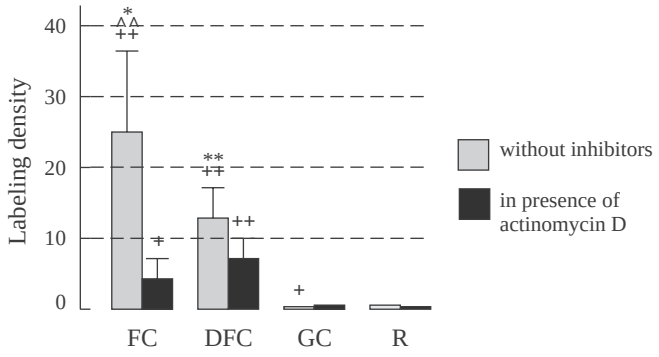

Fig. 3. Effect of actinomycin D upon BrUTP incorporation. Densities (gold particles/μm^2) on the FC, DFC, GC and resin (R) were calculated in untreated and actinomycin-D-treated nucleoli incubated with BrUTP for 10 minutes. The results represent mean values±s.e.m. 13 and 8 random micrographs were analyzed and 211 and 47 gold particles were counted, respectively. Student's *t*-test for nucleolar components versus resin (+ P<0.05, ++ P<0.01) for each nucleolar component in untreated versus treated nucleoli (* P<0.05, ** P<0.01) and for FC versus DFC in untreated or treated nucleoli (^ P<0.05, ^^ P<0.01) was used.

incorporation. When cordycepin was present throughout the experiment (Fig. 5), BrUTP incorporation was significantly reduced, and only 20% of nucleoli were labelled. The labelling density on both the FC and the DFC, although still significant, was very low. After a cordycepin pretreatment, 82% of nucleoli incorporated BrUTP (relative to 89% in control experiments without cordycepin). In these experimental conditions, the FC displayed high labelling density (Fig. 5B,C), which was significantly higher than that of the FC of control nucleoli labelled in the absence of cordycepin (Fig. 5A,C).

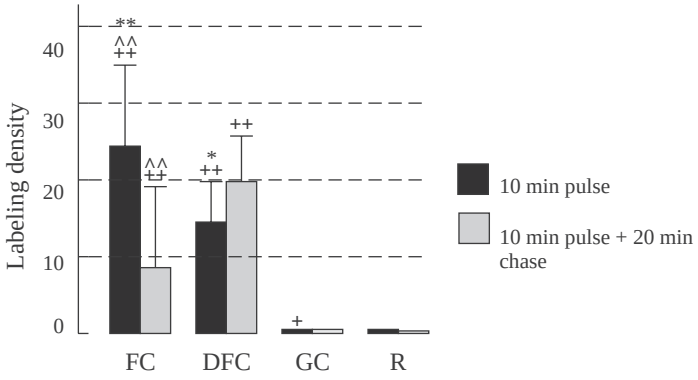

Fig. 4. Immunogold detection of BrUTP-labelled rRNAs on ultrathin sections of isolated nucleoli from ELT cells pulse-labelled for 10 minutes with BrUTP and pulse-labelled for 10 minutes with BrUTP followed by a 20 minute chase with UTP. Densities (gold particles/μm^2) on the FC, DFC, GC and resin (R) were calculated in both cases. The results shown represent means±s.e.m. 13 and 25 random micrographs were analyzed, and 306 and 420 gold particles were counted, respectively. Student's *t*-test for nucleolar components versus resin (+ P<0.05, ++ P<0.01) for each nucleolar component in pulse-labelled versus pulse-labelled and chased nucleoli (* P<0.05, ** P<0.01) and for FC versus DFC in pulse-labelled or pulse-labelled and chased nucleoli (^ P<0.05, ^^ P<0.01) was used.

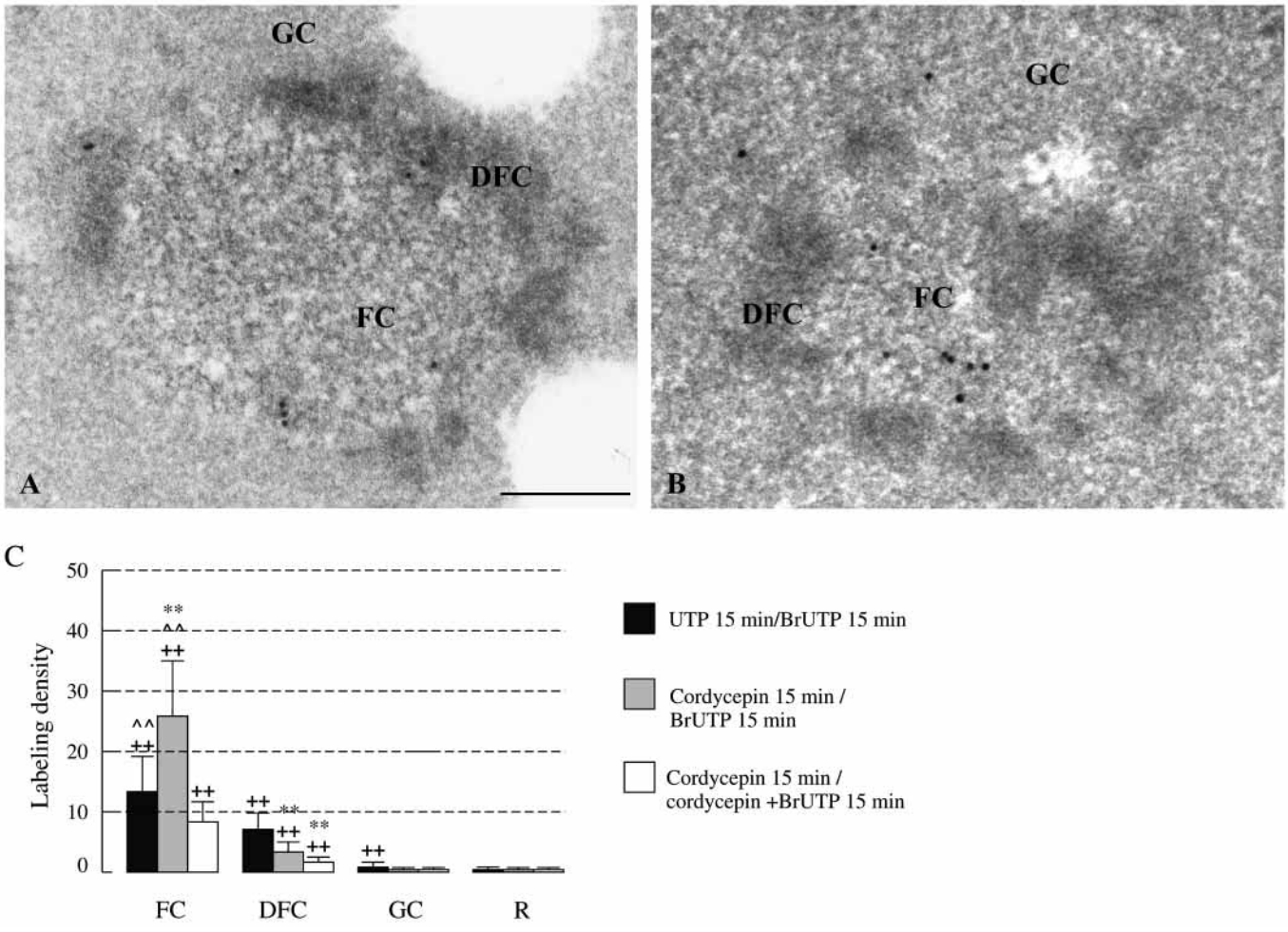

Fig. 5. Ultrastructural identification of initiation sites of rDNA transcription within the nucleolus. (A,B) Immunogold detection of BrUTP-labelled rRNAs on ultrathin sections of isolated nucleoli from ELT cells, pulse-labelled for 15 minutes with BrUTP after a 15 minute incubation with transcription medium (A) or pulse-labelled for 15 minutes with BrUTP after a 15 minute incubation in the presence of an elongation inhibitor, cordycepin, instead of ATP (B). Bar, 0.25 μm. (C) Density (gold particles/μm^2) on the FC, DFC, GC and resin (R) in nucleoli isolated from ELT cells. The results represent means±s.e.m. 24, 24 and 14 random micrographs were analyzed and 464, 381 and 141 gold particles were counted, respectively. Student's *t*-test for nucleolar components versus resin (+ P<0.05, ++ P<0.01) for each nucleolar component in untreated versus treated nucleoli (* P<0.05, ** P<0.01) and for FC versus DFC in untreated or treated nucleoli (^ P<0.05, ^^ P<0.01) was used.

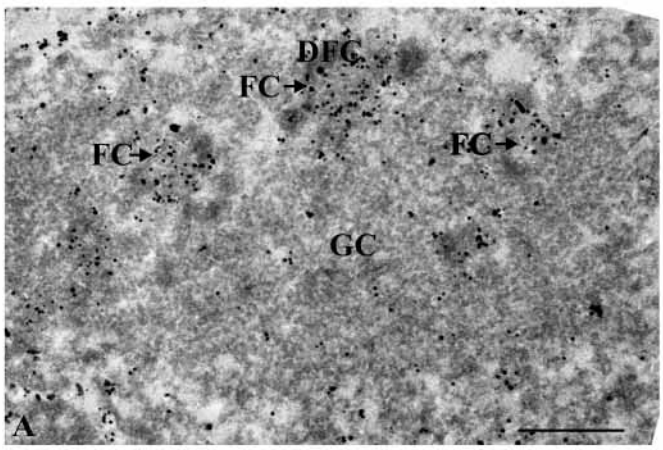

Fig. 6. Ultrastructural localization of RNA polymerase I within A549 cells. Anti-RPI antibodies were revealed with fluoronanogold, followed by silver enhancement. After embedding, ultrathin sections (80 nm) were counterstained and observed with an electron microscope at 100 kV. The main nucleolar components are identified (FC, DFC and GC). A high density of particles is observed within the fibrillar components of the nucleolus. Bar, 0.5 μm.

Three-dimensional distribution of RPI

In order to study the volumic organization of RPI, immunolabelling was performed in A549 cells before embedding. First, the localization of the whole labelling relatively to the ultrastructure was checked by producing ultrathin sections counterstained with lead and uranyl. This revealed a preserved nucleolar ultrastructure (Fig. 6) in which several FCs (~270 nm in diameter) were identified as the sites where most silver particles were found.

From similar preparations, 500 nm thick sections were produced. Under observation at 250 kV, RPI labelling always appeared as several discrete clusters of particles in which the density of the labelling is 10 times higher than that of the nucleoplasm (data not shown). The clusters are organized as spheroids ~270 nm in diameter (Fig. 7A). They contained ~150 individualized silver particles and displayed a similar volumic organization. The cluster framed in Fig. 7A was taken as a representative example. By rotating the tomogram at different angles, it was possible to reveal all the details of the structure and choose the most pertinent and demonstrative views. The particles presented a highly organized structure within a cluster, as evidenced by a rotation at +15° (Fig. 7D). This view revealed that the cluster is composed of several coils, 60 nm in diameter, as also seen on a stereopair displayed with a surfacic rendering mode (Fig. 7E). Rotations and complex spatial moving around this reconstructed object were performed to determine the number of coils, to measure their length and to investigate their spatial organization (movie abailable at jcs.biologists.org/supplemental). Three curved coils (150-200 nm in length, #1-3) and two shorter ones (30-50 nm in length, numbers 4 and 5) were observed (Fig. 7D). These coils share a common origin (Fig. 7D,I, circles) but display separate extremities (brackets).

In order to investigate the internal arrangement of RPI within the FC, 30 nm thick coronal sections were computed from the tomogram displayed in Fig. 7D (Fig. 7F-I). Notably, the central region is devoid of particles (asterisks). The coronal sections revealed the internal structure of the coils, in which RPI particles were frequently aligned to form 20 nm thick twines with a free terminal end (Fig. 7G-I, arrows). To further investigate their orientation, the volume was rotated to place the coils in a vertical position, and a sectioning plane parallel to the axis of coil number 2 was applied (Fig. 8A,B). In these conditions, two successive, 1.5 nm thick sections revealed seven twines, which were orthogonally disposed relatively to the axis of the coil and were parallel to each other [Fig. 8A,B, arrows; Movie 2 (available at jcs.biologists.org/supplemental)]. When 1.5 nm thick sections were produced perpendicularly to the axis of the coil, it appeared that the twines formed full or partially open circles, 60 nm in diameter [Fig. 8C,D, white circles; Movie 3 (available at jcs.biologists.org/supplemental)]. These features were also evidenced on a three-dimensional visualization performed on one half of the volume [Fig. 8E; Movie 4 (available at jcs.biologists.org/supplemental)].

Number of active rDNA genes per fibrillar center

DRB treatment was used to estimate the number of active rDNA genes per transcription site. DRB unravels nucleolar components and the fibrillar components (FC and DFC) form separate beads, each of which containing a single rDNA gene (Haaf et al., 1991). After UBF immunostaining, a marker of both FC and DFC, a series of optical sections in control and DRB-treated cells were produced and analyzed by confocal microscopy. In control cells, UBF staining appeared as frequently superimposed dots within the whole nucleolar volume, whereas in treated cells, UBF was found within discrete dots, arranged as extended necklaces. Whole projections were then calculated and a quantification led to 89 (±16) and 180 (±25) dots for 12 control and 12 treated cells, respectively. The value obtained for control cells was probably underestimated because of the relatively low resolution of the confocal microscope on the z-axis (0.4 μm) compared with the size of the dots (0.3 μm). These results indicate that in control cells, most transcription sites contain either a single active rDNA copy or two rDNA copies seen as two distinct clusters arranged in close proximity.

Discussion

In this study, we used two approaches to address the question of how 6 μm long ‘Christmas trees’ (i.e. transcribing rRNA genes) are organized in the nucleolus. First, we attempted to identify the nucleolar compartment(s) in which the initial sites of BrUTP incorporation are located. In order to work with a model in which transcription is slowed down, we used nucleoli that were isolated by a method that preserves their morphological integrity (Vandelaer et al., 1996). In addition, we chose ELT cells, which contain large FCs, to increase the accuracy of our quantifications on ultrathin sections. Since images obtained by electron microscopy are two-dimensional projections, the precision of the localization of a given labelling is higher if the diameter of the FCs is large (Thiry and Goessens, 1996). The transcriptional rate, ascertained by a time course of [^{3}H]-GTP and/or BrUTP incorporation, gave results comparable to those obtained previously in permeabilized human bladder carcinoma and HeLa cells

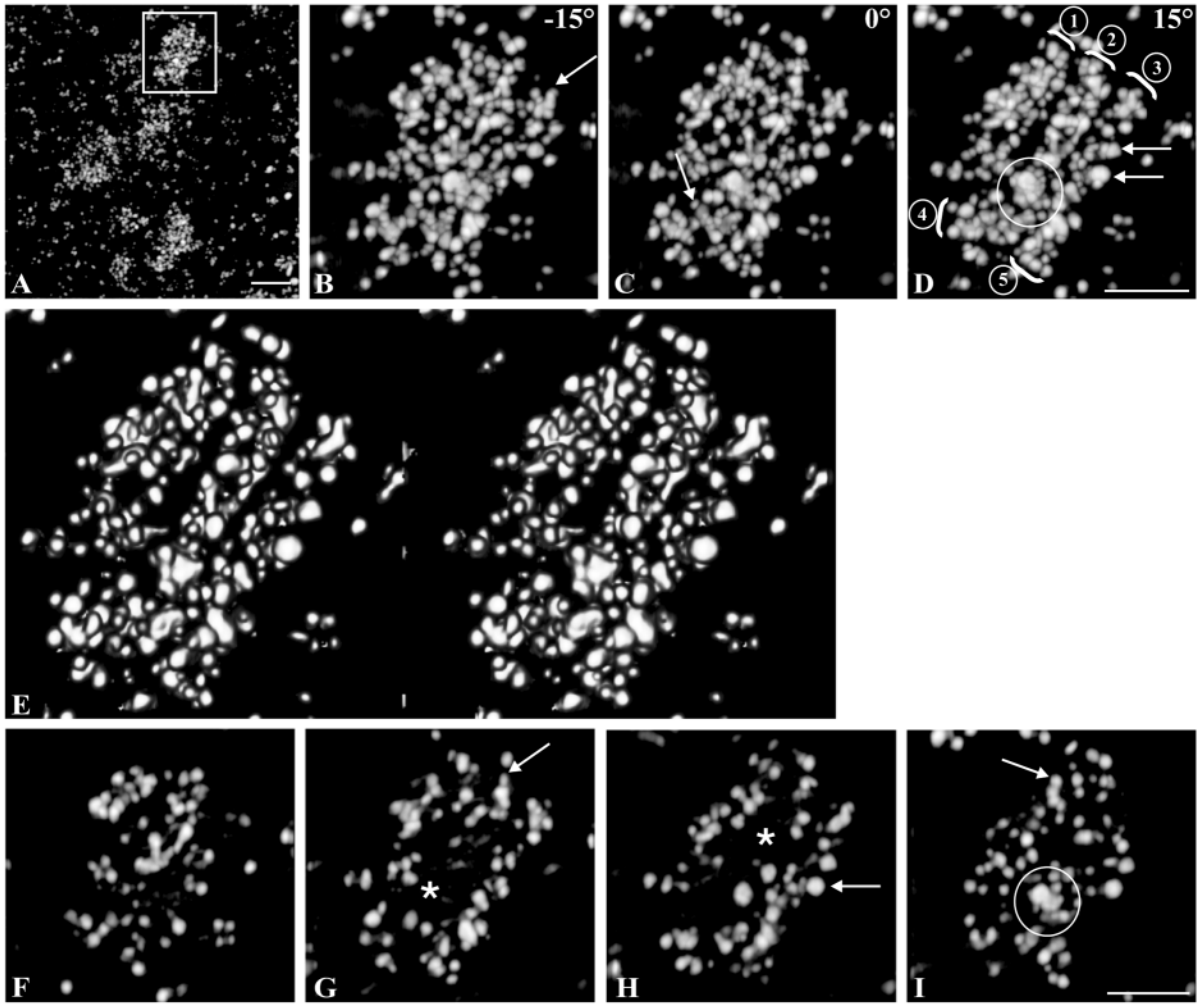

Fig. 7. Tomographic study of A549 cells immunolabelled with anti-RNA polymerase I antibodies. Contrast was inverted so that silver particles appear white. A 500 nm thick section observed using a STEM working at 250 kV is displayed: several independent clusters, 270 nm in diameter, are seen (A). (B-D) Different projections of the tomogram were calculated after tomographic reconstruction of the cluster framed in (A). At +15° (D), five 60 nm coils are seen, as indicated by brackets numbers 1 to 5. The large circle shows the area where the coils are fused together. The arrows point to twines, 20 nm in thickness. (E) A stereopair of the tomogram presented in the same orientation as in (D) was calculated thanks to a surfacic rendering mode. (F-I) Four successive 30 nm thick sections were achieved with a coronal orientation within the tomogram presented in (D). Asterisks (G,H) indicate the internal part of the cluster, devoid of labelling, and arrows (G,I) refer to twines. Bar, 200 nm (A) or 100 nm (B-I).

(Jackson et al., 1993; Wansink et al., 1993). As shown by run-on assays, incorporation of BrUTP in isolated nucleoli reached a plateau at 8 minutes that is maintained for 30 minutes. This is in agreement with previous in vitro experiments (Grummt, 1978). Consequently, incubation times in the range of 10-30 minutes were chosen for the following experiments. Our data indicate that BrUTP incorporation in the FC and DFC is the result of RPI activity, as proved by transcriptional inhibition with actinomycin D (Fig. 3).

With this in vitro system, nascent transcripts are mainly detected in the FC and to a lesser extent in the DFC. This observation correlates with previous in vivo studies showing that the first sites to be labelled by BrUTP in lipofected cells are the FC and the DFC (Thiry et al., 2000), but it does not agree with experiments using BrUTP incorporation within permeabilized cells (Hozak et al., 1994) or BrUTP introduced by microinjection (Cmarko et al., 1999). To explain this discrepancy, the dynamics of nascent rRNAs must be taken into account. In order to analyze their migration, we performed pulse-chase experiments (Fig. 4). Our data showed a significant decrease of the labelling in the FC and a simultaneous increase in the DFC. This demonstrates that the FC is the site of primary BrUTP incorporation and that the pre-rRNAs enter within the surrounding DFC during the elongation process. Moreover, the primary sites of BrUTP incorporation were identified after a transient inhibition of elongation by cordycepin, whose action leads to premature transcriptional termination (Siev et al., 1969; Suhadolnik, 1979), thus allowing new RPI molecules to be engaged in transcription immediately after the release of inhibition. Upon transcription reactivation, a subsequent BrUTP pulse initiated preferential labelling of the FCs, whereas DFC-specific labelling was very low (Fig. 5). This

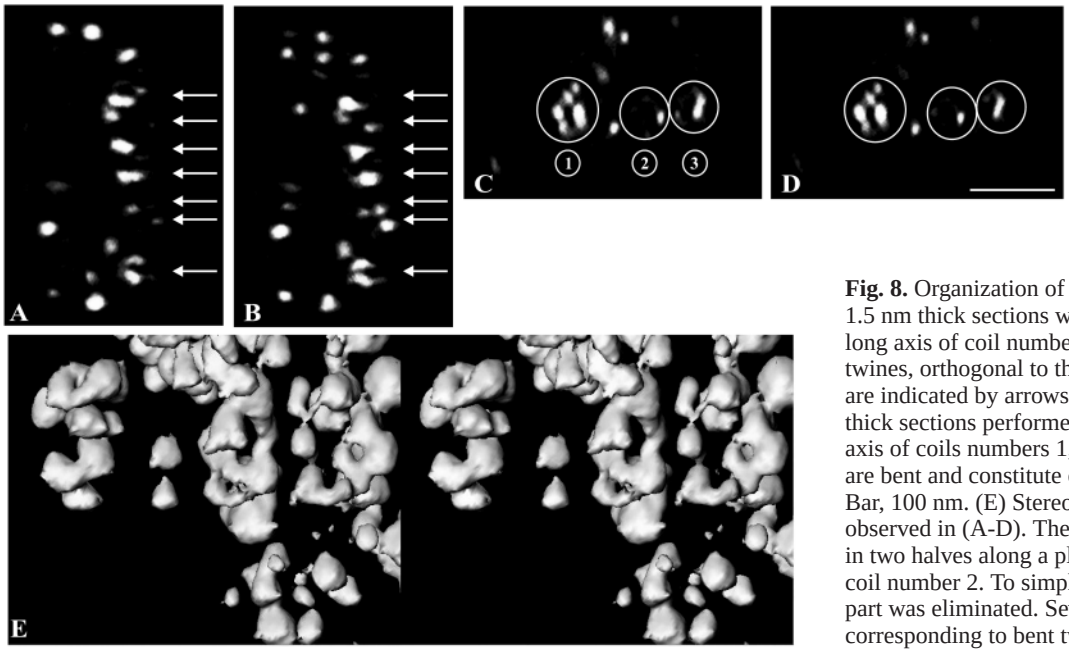

Fig. 8. Organization of the coils. (A,B) Two successive 1.5 nm thick sections were produced parallel to the long axis of coil number 2. The positions of seven twines, orthogonal to the long axis of coil number 2, are indicated by arrows. (C,D) Two successive 1.5 nm thick sections performed perpendicularly to the long axis of coils numbers 1, 2 and 3. Twines (large circles) are bent and constitute closed or partially open circles. Bar, 100 nm. (E) Stereo-pair showing the twines observed in (A-D). The volume of the cluster was cut in two halves along a plane parallel to the long axis of coil number 2. To simplify the visualization, the rear part was eliminated. Several open and closed circles corresponding to bent twines can be seen.

finding demonstrates that the FCs are the sites of rDNA transcription within the nucleolus. Taken together, these experiments demonstrate that transcription of rDNA genes takes place in the cortex of FC and that growing rRNA rapidly enter the DFC. This is consistent with the results of previous work in which RPI have been located exclusively or preferentially in the FCs (Scheer and Rose, 1984; Reimer et al., 1987; Raska et al., 1989). Moreover, other studies have found DNA, including rDNA genes, in the FCs, preferentially in their cortical part (Thiry and Thiry-Blaise, 1989; Puvion-Dutilleul et al., 1991; Thiry and Thiry-Blaise, 1991; Thiry et al., 1993) and also small amounts of nascent RNAs over the FCs themselves (Goessens, 1976; Thiry et al., 1985; Dupuy-Coin et al., 1986; Derenzini et al., 1987; Thiry and Goessens, 1991; Thiry et al., 2000).

We also addressed the question of the volumic organization of the transcription machinery by performing electron tomography on cells immunolabelled with anti-RPI antibodies prior to embedding. This technique is the only one that can reveal the distribution of labelled particles within a cellular volume at the electronic level (Koster et al., 1997; McEwen and Marko, 2001). A549 cells were chosen because they contain numerous FCs, whose small size (~0.27 μm in diameter) allows them to be fully contained within the section thickness (0.5 μm). In addition, FCs of A549 cells are homogenous in size, in contrast to ELT cells. This factor was essential to allow structural comparisons between the different FCs analyzed in the present study. Since antigen detection represents a critical parameter for tomographic studies, we performed a fixation with paraformaldehyde and a mild permeabilization with Triton X-100 to achieve the best compromise between antigen accessibility and ultrastucture preservation (Humbel et al., 1998). Similarly, fluoronanogold was chosen for its reduced size, which facilitates its penetration within the specimen and reveals antigens, unlike 5 or 10 nm gold particles, which are unable to penetrate (Robinson et al., 2000). Moreover, the use of fluoronanogold before embedding increases significantly the sensitivity of antigen detection compared with classic methods using 5 to 10 nm gold particles on the surface of ultrathin sections (Hainfeld and Furaya, 1992; Hainfeld and Powell, 2000). Finally, silver amplification was controlled by using a protective colloid that favoured the growth of silver particles centred on the gold clusters in order to reveal the exact location of antigens (Baschong and Stierhof, 1998). The relevance of this detection procedure has been demonstrated previously (Robinson and Vandré, 1997), using pre-embedding immunolabelling of tubulin in leukocytes. Robinson and Vandré observed 25 nm thick fibres that correspond almost exactly to the size of microtubules, which indicates that fluoronanogold reveals the exact size of structures containing antigens.

As shown previously, the observation of counterstained ultrathin sections demonstrated that the RPI molecules are mainly localized within the FC (Scheer and Rose, 1984; Reimer et al., 1987; Raska et al., 1989). The detection of RPI before embedding led to a labelling density that was significantly higher than that observed classically on ultrathin sections (Fig. 6). This can be explained by both the sensitivity of the detection (see above) and the fact that the antigens were observed throughout the thickness of the section (80 to 100 nm), unlike conventional detection protocols that only reveal antigens located at its surface. In addition to a strong labelling in the FCs, a weak RPI labelling was also seen in the GC. Interestingly, a similar distribution of RPI was obtained by STEM analyses performed on sections containing whole FCs (i.e. 0.5 μm in thickness), followed by three-dimensional reconstructions (Fig. 7A). Indeed, the main sites of RPI labelling are organized into discrete clusters, clearly separated from one another and surrounded by a much weaker labelling. The coincidence of ultrastructural analyses and three-dimensional data allows us to conclude that RPI clusters are located in the FCs. Quantification showed that the labelling density of RPI was 90% in the clusters and 10% in their environment. This view, although seen at a much higher

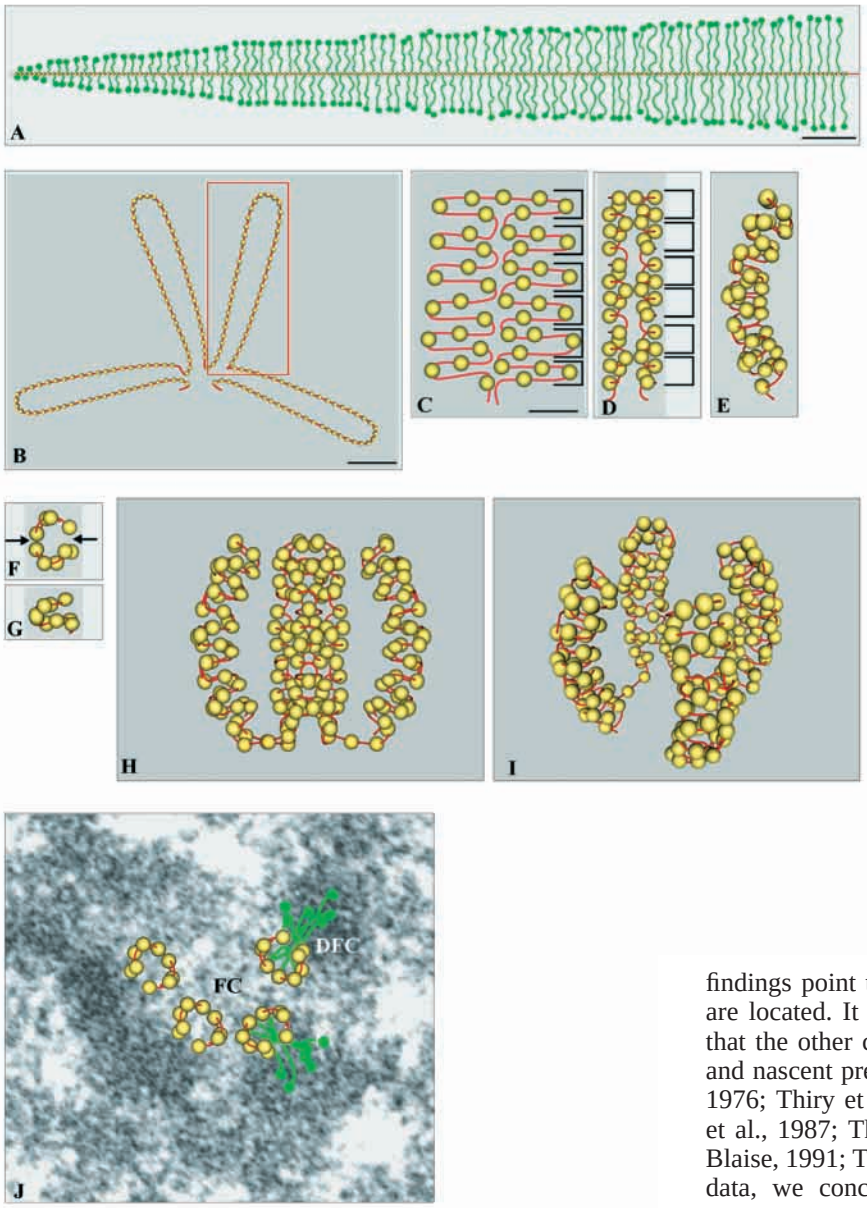

Fig. 9. A model of the three-dimensional organization of an active rDNA gene within a fibrillar center. (A) Spread of a 'Christmas tree' drawn at scale. (B) For simplicity, only the rDNA gene covered with 180 RPI molecules is presented; it is folded into four identical loops. (C) Each loop (boxed in B) folds into a separate coil. It consists of two identical rows (200 nm in length) of small loops (60 nm in length) (brackets) that are covered with 3-4 RPI molecules. (D,E) A coil is obtained by bending the small loops on the matrix of a cylinder, 60 nm in diameter and 200 nm in length. In this case, it is composed of a stack of six open rings, 30 nm in thickness (brackets on D). (F,G) Upper and side views of a ring: each ring is composed of two twines, 60 nm long; the arrows in (F) point to the two openings of a ring. (H,I) For convenience, the whole length of a rDNA gene has been wrapped into four identical coils (H, side view; I, perspective view). Experimentally, each cluster was composed of three to five coils, whose lengths were variable. In our model, this disparity could be taken into account by placing more (or less) rings in each coil. (J) A classically stained, ultrathin section was merged with a cross-section of the model shown in (H and I) at the same scale. Cross-sections of the coils, localized within the cortex of FC, appear as open rings without rRNA molecules (on the left) or with elongating rRNAs molecules emerging from the convex face of the coil and entering the surrounding DFC. Bar, 400 nm (A), 100 nm (B) and 50 nm (C-J).

resolution, is in agreement with the picture of GFP-tagged nucleolar proteins observed by confocal microscopy, showing main nucleolar sites surrounded by a weaker labelling (Phair and Misteli, 2000; Chen and Huang, 2001; Savino et al., 2001). FRAP experiments have proved that this pattern reflects the rapid exchange of nucleolar proteins between their nucleolar binding sites and the nucleoplasm (Phair and Misteli, 2000; Chen and Huang, 2001).

Several lines of evidence indicate that the three-dimensionally organized clusters are the sites at which transcribing RPI molecules are located. However, the question of whether the clusters are composed of transcriptionally active or inactive molecules cannot be answered, as at the present time no antiserum or modification can discriminate between these two states. First, the localization of RPI relative to the ultrastructure shows that RPI is predominantly found in the FCs. In the present study, the FCs were further identified as the initial sites where BrUTP incorporation takes place. These findings point to the FCs as the sites where transcribing RPI are located. It corroborates numerous other studies, showing that the other counterparts of RPI transcription, rDNA genes and nascent pre-rRNAs, are also found in the FCs (Goessens, 1976; Thiry et al., 1985; Dupuy-Coin et al., 1986; Derenzini et al., 1987; Thiry and Thiry-Blaise, 1989; Thiry and Thiry-Blaise, 1991; Thiry et al., 1993; Thiry et al., 2000). From these data, we conclude that the FCs are the sites where RPI transcription occurs. We addressed the question of the number of rDNA genes that are present in each FC. Our experiments using DRB treatment on A549 cells revealed that most FCs contain a single active rDNA gene, which is in agreement with previous results obtained from highly proliferating cells (Ochs and Smetana, 1989).

From the tomographic analyses of 16 different tomograms, the structure of each cluster was further described, and it revealed two levels of organization. First, several coils, displaying a common origin, showed a spatial arrangement recalling that of a corolla, as confirmed by the presence of a central cavity. Second, the internal organization of the coils revealed bent twines, approximately 60 nm long and 20 nm thick. We hypothesize that the coils are constituted with RPI molecules engaged on the rDNA gene and that their spatial distribution can be used to propose a model for the three-dimensional organization of the rDNA gene in situ (Fig. 9). Using images of spreads, the transcribed region of a mammalian rDNA gene (~6000 nm in length) was considered to be covered with 30 RPI molecules/μm (Trendelenburg and

Puvion-Dutilleul, 1987). The size of a RPI molecule was estimated to 16 nm, and the length of fully elongated rRNAs to be 350 nm (these pre-rRNAs molecules being 3 nm in diameter and ending with a 20 nm wide particle) (Fig. 9A). Our data, which revealed four to five coils emanating from a common origin, can be correlated with previous results showing the presence of matrix-associated regions both in the 5′NTS and in the 3′NTS of rDNA genes (Stephanova et al., 1993). Moreover, the termination transcription factor TTF1, which can oligomerize and form aggregates, binds both to the initiation and the termination sites of rDNA genes, thus organizing each rDNA gene as a loop (Reeder and Lang, 1997). These results were schematized by folding the rDNA gene into four loops (Fig. 9B), each of which undergoes another level of folding, thus forming two parallel rows (Fig. 9C). These rows (~200 nm in length) consist of successive small loops (brackets), ~60 nm in length, each of which contains three to four RPI molecules. The bending of all the loops on the matrix of a cylinder produces a coil, 60 nm in diameter and 200 nm in length (Fig. 9D,E), similar to those observed after RPI immunolabelling. Consequently, a coil could be obtained by stacking about six open rings (brackets on D), each of which are constituted as two twines (Fig. 9F,G). These views are in agreement with the transversal and longitudinal sections of the coils (Fig. 8). The high level of bending and looping needed in this model could be performed by UBF, a very abundant nucleolar protein. Indeed, UBF has the ability to bend rDNA (Putnam et al., 1994), and its binding is not restricted to the regulatory sequences of the ribosomal DNA repeats, but it can occur all along these sequences (O'Sullivan et al., 2002).

Finally, a transcribed rDNA gene can be spatially organized within a limited volume as four similarly organized coils (Fig. 9H,I), with a compaction factor of approximately seven. This model still allows enough spacing between RPI molecules and rDNA for pre-rRNAs molecules to be elongated without steric hindrance. The openings of the rings (arrows on Fig. 9F) give rise to two longitudinal grooves along each coil, which can be observed in the rotation of the whole model (Movie 5, available at jcs.biologists.org/supplemental). A transverse section of the figure presented in Fig. 9H (270 nm in diameter) fits within a FC, as represented at the same magnification on an ultrathin section (Fig. 9J). Our BrUTP incorporation data, which demonstrate that growing pre-rRNAs molecules are synthesized in the FC and enter the surrounding DFC, have been schematized on Fig. 9J as polarized threads. It illustrates, by using in vivo BrUTP incorporation and classic post-embedding detection methods, why the probability of finding BrUTP over the DFC is very high and why a slowed-down system is a prerequisite to observe BrUTP on the FC. Our model supposes the positioning of the growing rRNA extremities in two different compartments, which is supported by the finding that pre-rRNAs are in a extended conformation during transcription (Stanek et al., 2001)

Our model correlates with the fact that the presence of the DFC in the nucleolus is critically dependent on ongoing transcription of the rRNA genes. Microinjection of anti-RPI antibodies reduces rRNA synthesis (Schlegel et al., 1985). It also modifies the nucleolar morphology: the DFC is rapidly disorganized after microinjection and forms extra-nucleolar bodies that are devoid of RPI (Benavente et al., 1988). Moreover, after hypotonic shock leading to a complete reorganization of the nucleolar structures, the FCs and the DFCs are totally separated and rDNA is only found in the remains of the FCs (Zatsepina et al., 1997). The intimate association of the FCs with the DFC might provide a structural framework that maintains transcriptional products in a specific topological order, which is necessary for the subsequent cascade of maturation and processing steps.

Finally, this model allows the juxtaposition of several active genes, whose association would then form larger FCs. This could account the difference in sizes of FCs from different cellular models. Further tomographic studies performed on FCs from various cell lines will be necessary to assess this hypothesis.

This work was supported by grants from ARERS, the Ligue Régionale de l'Aube and Association pour la Recherche sur le Cancer (Grant No. 4497) to D.P. and from 'Fonds de la Recherche Scientifique Médicale' (Grant No. 3.4578.98) to M.T. T.C. was a fellow of Association pour la Recherche sur le Cancer. M.T. is a research associate of the National Fund for Scientific Research (Belgium). The authors are grateful to K. Rose for the generous gift of anti-RPI antibodies. Thanks are also due to Francine Skivée for technical assistance, to David Ploton for construction of the model and to Guy Goessens and M. O'Donohue for their critical reading of the manuscript.

References

Bahr, G. F., Boccia, J. A. and Engler, W. F. (1979). Reconstruction of a chromosome model from its projections. *Ultramicroscopy* **4**, 45-53.

Baschong, W. and Stierhof, Y. D. (1998). Preparation, use and enlargement of ultrasmall gold particles in immunoelectron microscopy. *Microsc. Res. Tech.* **42**, 66-79.

Baumeister, W., Grimm, R. and Walz, J. (1999). Electron tomography of molecules and cells. *Trends Cell Biol.* **9**, 81-85.

Benavente, R., Reimer, G., Rose, K. M., Hugle-Dorr, B. and Scheer, U. (1988). Nucleolar changes after microinjection of antibodies to RNA polymerase I into the nucleus of mammalian cells. *Chromosoma* **97**, 115-123.

Beorchia, A., Héliot, L., Ménager, M., Kaplan, H. and Ploton, D. (1992). Applications of medium-voltage STEM for the 3-D study of organelles within thick sections. *J. Microsc.* **170**, 247-258.

Biggiogera, M., Malatesta, M., Abolhassani-Dadras, S., Amalric, F., Rothblum, L., and Fakan, S. (2001). Revealing the unseen: the organizer region of the nucleolus. *J. Cell Sci.* **114**, 3199-3205.

Bréchard, M. P., Hartung, M., de Lanversin, A., Cau, P. and Stahl, A. (1994). Localization of rDNA transcription sites in nucleoli of human Sertoli cells by EM quantitative autoradiographic study using ^{3}H-uridine. *Biol. Cell* **81**, 247-256.

Chen, D. and Huang, S. (2001). Nucleolar components involved in ribosome biogenesis cycle between the nucleolus and nucleoplasm in interphase cells. *J. Cell Biol.* **153**, 169-176.

Cmarko, D., Verschure, P. J., Martin, T. E., Dahmus, M. E., Krause, S., Fu, X. D., van Driel, R. and Fakan, S. (1999). Ultrastructural analysis of transcription and splicing in the cell nucleus after bromo-UTP microinjection. *Mol. Biol. Cell* **10**, 211-223.

Crowther, R. A., de Rosier, D. J. and Klug, A. (1970). The reconstruction of a three-dimensional structure from projections and its application to electron microscopy. *Proc. R. Soc. Lond. Ser. A* **317**, 319-340.

Derenzini, M., Hernandez-Verdun, D., Farabegoli, F., Pession, A. and Novello, F. (1987). Structure of ribosomal genes of mammalian cells *in situ*. *Chromosoma* **95**, 63-70.

Derenzini, M., Thiry, M. and Goessens, G. (1990). Ultrastructural cytochemistry of the mammalian cell nucleus. *J. Histochem. Cytochem.* **38**, 1237-1256.

Dundr, M. and Raska, I. (1993). Nonisotopic ultrastructural mapping of transcription sites within the nucleolus. *Exp. Cell Res.* **208**, 275-281.

Dupuy-Coin, A. M., Pebusque, M. J., Seite, R. and Bouteille, M. (1986). Localization of transcription in nucleoli of rat sympathetic neurons. A quantitative ultrastructural autoradiography study. *J. Submicrosc. Cytol.* **18**, 21-27.

Fakan, S. (1978). High resolution autoradiography studies on chromatin functions. In *The Cell Nucleus* (ed. H. Busch), pp. 3-53. New York: Academic Press.

Goessens, G. (1976). High resolution autoradiographic studies of Ehrlich tumour cell nucleoli. *Exp. Cell Res.* **100**, 88-94.

Grummt, I. (1978). *In vitro* synthesis of pre-rRNA in isolated nucleoli. In *The Cell Nucleus* (ed. H. Busch), pp. 373-414. New York: Academic Press.

Haaf, T., Hayman, D. L. and Schmid, M. (1991). Quantitative determination of rDNA transcription units in vertebrate cells. *Exp. Cell Res.* **193**, 78-86.

Hadjiolov, A. A. (1985). Ribosomal genes. In *The Nucleolus and Ribosome Biogenesis* (ed. A. A. Hadjiolov), pp. 5-51. Wien, Austria: Springler Verlag.

Hainfeld, J. F. and Furuya, F. R. (1992). A 1.4-nm gold cluster covalently attached to antibodies improves immunolabeling. *J. Histochem. Cytochem.* **40**, 177-184.

Hainfeld, J. F. and Powell, R. D. (2000). New frontiers in gold labeling. *J. Histochem. Cytochem.* **48**, 471-480.

Héliot, L., Kaplan, H., Lucas, L., Klein, C., Beorchia, A., Doco-Fenzy, M., Ménager, M., Thiry, M., O'Donohue, M. F. and Ploton, D. (1997). Electron tomography of metaphase nucleolar organizer regions: evidence for a twisted-loop organization. *Mol. Biol. Cell* **8**, 2199-2216.

Hozak, P., Cook, P. R., Schöfer, C., Mosgöller, W. and Wachtler, F. (1994). Site of transcription of ribosomal RNA and intranucleolar structure in HeLa cells. *J. Cell Sci.* **107**, 639-648.

Humbel, B. M., de Jong, M. D. M., Müller, W. H. and Verkleij, A. J. (1998) Pre-embedding immunolabeling for electron microscopy: an evaluation of permeabilization methods and markers. *Microsc. Res. Tech.* **42**, 43-58.

Jackson, D. A., Hassan, A. B., Errington, R. J. and Cook, P. R. (1993). Visualization of focal sites of transcription within human nuclei. *EMBO J.* **12**, 1059-1065.

Klein, C., Cheutin, T., O'Donohue, M. F., Rothblum, L., Kaplan, H., Beorchia, A., Lucas, L., Héliot, L. and Ploton, D. (1998). The three-dimensional study of chromosomes and of UBF-immunolabelled NORs demonstrates their non-random spatial arrangement during mitosis. *Mol. Biol. Cell* **9**, 3147-3159.

Koster, A. J., Grimm, R., Typke, D., Hegerl, R., Stoschek, A., Walz, J. and Baumeister, W. (1997). Perspectives of molecular and cellular electron tomography. *J. Struct. Biol.* **120**, 276-308.

Le Negrate, A., Beghdadi, A. and Dupoisot, H. (1992). An image enhancement technique and its evaluation through bimodality. *Comp. Vis. Graph.* **54**, 13-22.

Lepoint, A. and Bassleer, R. (1978). Number of nucleoli in Ehrlich tumor cells during interphase. V*irchows Arch. B. Cell Path.* **26**, 267-273.

McEwen, B. F. and Marko, M. (2001). The emergence of electron tomography as an important tool for investigating cellular ultrastructure. *J. Hist. Cytochem.* **49**, 553-563.

Mélèse, T. and Xue, Z. (1995). The nucleolus: an organelle formed by the act of building a ribosome. *Curr. Biol.* **7**, 319-324.

Miller, O. L. and Beatty, B. R. (1969). Visualization of nucleolar genes. *Science* **164**, 955-957.

Moss, T. and Stefanovsky, V. (1995). Promotion and regulation of ribosomal transcription in eukaryotes by RNA polymerase I. *Prog. Nucl. Acid Res. Mol. Biol.* **50**, 25-66.

Ochs, R. L. and Smetana, K. (1989). Fibrillar center distribution in nucleoli of PHA-stimulated human lymphocytes. *Exp. Cell Res.* **184**, 552-557.

Olson, M. O., Dundr, M. and Szebeni, A. (2000). The nucleolus: an old factory with unexpected capabilities. *Trends Cell Biol.* **10**, 189-196.

O'Sullivan, A., Sullivan, G. and McStay, B. (2002). UBF binding in vivo is not restricted to regulatory sequences within the vertebrate ribosomal DNA repeat. *Mol. Cell. Biol.* **22**, 657-668.

Phair, R. D. and Misteli, T. (2000). High mobility of proteins in the mammalian cell nucleus. *Nature* **404**, 604-609.

Putnam, C. D., Copenhaver, G. P., Denton, M. L. and Pikaard, C. S. (1994). The RNA polymerase I transactivator upstream binding factor requires its dimerization and high-mobility-group (HMG) box 1 to bend, wrap, and positively supercoil enhancer DNA. *Mol. Cell. Biol.* **14**, 6476-6488.

Puvion-Dutilleul, F., Mazan, S., Nicoloso, M., Christensen, M. E. and Bachellerie, J. P. (1991). Localization of U3 RNA molecules in nucleoli of HeLa and mouse 3T3 cells by high resolution in situ hybridization. *Eur. J. Cell Biol.* **56**, 178-186.

Raska, I., Reimer, G., Jarnik, M., Kostrouch, Z. and Raska, K. Jr (1989). Does the synthesis of ribosomal RNA take place within nucleolar fibrillar centers or dense fibrillar components. *Biol. Cell* **65**, 79-82.

Reeder, R. H. and Lang, W. H. (1997). Terminating transcription in eukaryotes: lessons learned from RNA polymerase I. *Trends Biochem. Sci.* **22**, 473-477.

Reimer, G., Rose, K., Scheer, U. and Tan, E. (1987). Autoantibody to RNA polymerase I in *scleroderma sera*. *J. Clin. Invest.* **79**, 65-72.

Robinson, J. M. and Vandré, D. D. (1997). Efficient immunocytochemical labeling of eukocyte microtubules with fluoroNanogold: an important tool for correlative microscopy. *J. Hist. Cytochem.* **45**, 631-642.

Robinson, J. M., Takizawa, T. and Vandré, D. D. (2000). Enhanced labeling efficiency using ultrasmal immunogold probes: immunocytochemistry. *J. Hist. Cytochem.* **48**, 631-642.

Savino, T. M., Gébrane-Younès, J., de Mey, J., Sibarita, J. B. and Hernandez-Verdun, D. (2001). Nucleolar assembly of the rRNA processing machinery in living cells. *J. Cell Biol.* **153**, 1097-1110.

Scheer, U. and Rose, K. M. (1984). Localization of RNA polymerase I in interphase cells and mitotic chromosomes by light and electron microscopic immunocytochemistry. *Proc. Natl. Acad. Sci. USA* **81**, 1431-1435.

Scheer, U. and Hock, R. (1999). Structure and function of the nucleolus. *Curr. Opin. Cell Biol.* **11**, 385-390.

Schlegel, R. A., Miller, L. S. and Rose, K. M. (1985). Reduction in RNA synthesis following red cell-mediated microinjection of antibodies to RNA polymerase I. *Cell. Biol. Int. Rep.* **9**, 341-350.

Schöfer, C., Müller, M., Leitner, M. D. and Wachtler, F. (1993). The uptake of uridine in the nucleolus occurs in the dense fibrillar component. Immunogold localization of incorporated digoxigenin-UTP at the electron microscopic level. *Cytogenet. Cell. Genet.* **64**, 27-30.

Shaw, P. and Jordan, E. G. (1995). The nucleolus. *Annu. Rev. Cell Dev. Biol.* **11**, 93-121.

Siev, M., Weinberg, R. and Penman, S. (1969). The selective interruption of nucleolar RNA synthesis in HeLa cells by cordycepin. *J. Cell Biol.* **41**, 510-520.

Stanek, D., Koberna, K., Pliss, A., Malinsky, J., Masata, M., Vecerova, J., Risueno, M. C. and Raska, I. (2001). Non-isotopic mapping of ribosomal RNA synthesis and processing in the nucleolus. *Chromosoma* **110**, 460-470.

Stephanova, E., Stancheva, R. and Avramova, Z. (1993). Binding of sequences from the 5′- and 3′-nontranscribed spacers of the rat rDNA locus to the nucleolar matrix. *Chromosoma* **102**, 287-295.

Suhadolnik, R. J. (1979). Naturally occuring nucleoside and nucleotide antibodies. *Progr. Nucl. Acids Res. Mol. Biol.* **22**, 193-291.

Thiry, M. and Goessens, G. (1991). Distinguishing the sites of pre-rRNA synthesis and accumulation in Ehrlich tumor cell nucleoli. *J. Cell Sci.* **99**, 759-767.

Thiry, M. and Goessens, G. (1996). The Nucleolus during the Cell Cycle. In *Molecular Biology Intelligence Unit* (ed. R. G. Landes), pp. 1-144. Heidelberg, Germany: Springler-Verlag.

Thiry, M. and Thiry-Blaise, L. (1989). In situ hybridization at the electron microscope level: an improved method for precise localization of ribosomal DNA and RNA. *Eur. J. Cell Biol.* **50**, 235-243.

Thiry, M. and Thiry-Blaise, L. (1991). Locating transcribed and non-transcribed rDNA spacer sequences within the nucleolus by in situ hybridization and immunoelectron microscopy. *Nucleic Acids Res.* **19**, 11-15.

Thiry, M., Lepoint, A. and Goessens, G. (1985). Re-evaluation of the site of transcription in Ehrlich tumour cell nucleoli. *Biol. Cell* **54**, 57-64.

Thiry, M., Ploton, D., Ménager, M. and Goessens, G. (1993). Ultrastructural distribution of DNA within the nucleolus of various animal cell lines or tissues revealed by terminal deoxynucleotidyl transferase. *Cell Tissue Res.* **271**, 33-45.

Thiry, M., Cheutin, T., O'Donohue, M. F., Kaplan, H. and Ploton, D. (2000). Dynamics and three-dimensional localization of ribosomal RNA within the nucleolus. *RNA* **6**, 1750-1761.

Trendelenburg, M. and Puvion-Dutilleul, F. (1987). Electron microscopy in molecular biology, a practical approach (eds J. Sommerville and U. Scheer), pp. 101-146. Oxford, IRL Press.

Vandelaer, M., Thiry, M. and Goessens, G. (1996). Isolation of nucleoli from ELT cells: a quick new method that preserves morphological integrity and high transcriptional activity. *Exp. Cell Res.* **228**, 125-131.

Wansink, D.G., Schul, W., van Der Kraan, I., van Steensel, B., van Driel, R. and de Jong, L. (1993). Fluorescent labeling of nascent RNA reveals transcription by RNA polymerase II in domains scattered throughout the nucleus. *J. Cell Biol.* **122**, 283-293.

Weibel, E. R., Staubli, W., Gnagi, H. R. and Hess, F. A. (1969). Correlated morphometric and biochemical studies on the liver cell. I. Morphometric model, stereologic methods, and normal morphometric data for rat liver. *J. Cell Biol.* **42**, 68-91.

Zatsepina, O. V., Dudnic, O. A., Chentsov, Y. S., Thiry, M., Spring, H. and Trendelenburg, M. F. (1997). Reassembly of functional nucleoli following in situ unravelling by low-ionic-strength treatment of cultured mammalian cells. *Exp. Cell Res.* **233**, 155-168.